J. Am. Soc. Mass Spectrom. (2018) 29:260–269
DOI: 10.1007/s13361-017-1763-3

FOCUS: 32nd ASILOMAR CONFERENCE,
NOVEL INSTRUMENTATION IN MS AND ION MOBILITY: RESEARCH ARTICLE

A Linear Ion Trap with an Expanded Inscribed Diameter to Improve Optical Access for Fluorescence Spectroscopy

Vaishnavi Rajagopal, Chris Stokes, Alessandra Ferzoco

The Rowland Institute at Harvard University, Cambridge, MA 02142, USA

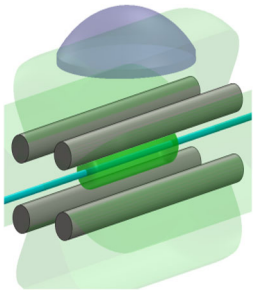

Abstract. We report a custom-geometry linear ion trap designed for fluorescence spectroscopy of gas-phase ions at ambient to cryogenic temperatures. Laser-induced fluorescence from trapped ions is collected from between the trapping rods, orthogonal to the excitation laser that runs along the axis of the linear ion trap. To increase optical access to the ion cloud, the diameter of the round trapping rods is 80% of the inscribed diameter, rather than the roughly 110% used to approximate purely quadrupolar electric fields. To encompass as much of the ion cloud as possible, the first collection optic has a 25.4 mm diameter and a numerical aperture of 0.6. The choice of geometry and collection optics yields 10^7 detected photons/s from trapped rhodamine 6G ions. The trap is coupled to a closed-cycle helium refrigerator, which in combination with two 50 Ohm heaters enables temperature control to below 25 K on the rod electrodes. The purpose of the instrument is to broaden the applicability of fluorescence spectroscopy of gas-phase ions to cases where photon emission is a minority relaxation pathway. Such studies are important to understand how the microenvironment of a chromophore influences excited state charge transfer processes.

Keywords: Fluorescence spectroscopy, Gas phase ion spectroscopy, Ion trap, Cryogenic, Excited state charge transfer

Received: 25 April 2017/Revised: 17 July 2017/Accepted: 18 July 2017/Published Online: 18 August 2017

Introduction

Both the dynamic and spectral properties of fluorescence emission are responsive to the microenvironment of a chromophore. The phenomenon, termed solvatochromism, is nicely demonstrated by the manifold of mutations of green fluorescence protein (GFP) [1–3] where the color of the emission of the same p-hydroxybenzylideneimidazolinone (HBI) chromophore is modulated by the surrounding protein scaffold from the blue Sirius (peak emission wavelength, $\lambda_{em,max}$ = 424 nm) [4] to yellow Citrine ($\lambda_{em,max}$ = 529 nm) [5]. When a model HBI chromophore is isolated in solution or the gas phase, removed from a protein environment, the fluorescence quantum yield is reduced by a factor of 10^3–10^4 [6–10].

While fluorescence provides a clear, visible demonstration of the effect of solvent on a chromophore, it should be expected that all excited state relaxation pathways are equally sensitive to the microenvironment. The system studied in most detail to date is excited state proton transfer from tert-butylamine to para-nitrophenyl-phenol [11, 12], for which it was shown that solvent fluctuations on the ground state and reorganization in the excited state were needed to explain the effect of isotopic substitution in the system. Excited state charge transfer is important to photosynthesis [13], enzymatic mechanisms [14], and radiation protection in the skin [15] and in DNA [16], and an understanding of the participation of the microenvironment is critical for the rational design of systems that mimic the function of these reactions.

In principle, studies of ions in the gas phase are a natural partner to fluorescence spectroscopy because of the ability to precisely control the solvation state of a chromophore. In practice, however, combining mass spectrometry with fluorescence spectroscopy presents technical challenges related to the low density of ions (weak signal) and the presence of scattering elements along the excitation laser path (high background). A typical density of ions in an ion trap is 10^6 molecules/cm^3 [17], which corresponds to fM concentrations in solution phase parlance. Even single molecule spectroscopists prefer to work with pM to nM concentrations (then ensure observation of only

Electronic supplementary material The online version of this article (doi:10.1007/s13361-017-1763-3) contains supplementary material, which is available to authorized users.

Correspondence to: Alessandra Ferzoco;
e-mail: ferzoco@rowland.harvard.edu

one fluorophore by restricting observations to a diffraction-limited volume) [18, 19].

Nevertheless, there are a number of areas of research that rely on the detection of fluorescence from gas-phase ions. The absorption cross-section of atomic ions is many orders of magnitude greater than that of molecules, so the field of trapped atomic ion fluorescence is more mature and has advanced to applications such as atomic clocks [20, 21] and quantum simulators [22, 23]. The first example of laser-induced fluorescence of a molecular ion was N_2^+ in 1975, concurrent with a flurry of measurements of ionization-induced fluorescence from organic radical cations [24]. However, the ions were neither trapped nor mass-selected [25]; that was first accomplished for CD^+ in a cylindrical ion trap in 1980 [26]. In the last decade or so, fluorescence spectroscopy of trapped gas-phase ions has been developed for non-volatile analytes, which provides an opportunity to expand the applicability of the technique [27–34].

Förster resonance energy transfer (FRET) studies of peptides, proteins, and oligonucleotides can provide structural information that is complementary to ion mobility, surface induced dissociation, and various other MS^n techniques [31, 35, 36]. Observing fluorescence quenching dynamics confers the added benefit of being able to observe temporally dynamic behavior [37], and excited state lifetime measurements can provide information about relative populations and their environment [38]. The types of questions addressed have primarily been structural in nature, and the types of compounds observed have been restricted to those where fluorescence is the primary relaxation pathway. Condensed phase spectroscopists, however, routinely utilize the spectral and temporal response of excited state emission to determine not only structure, but also for a comprehensive understanding of the chemical character, lifetime, and progression of excited states. In addition, the relatively high concentration of chromophores in condensed phase studies means emission can be used even when it is a minority relaxation pathway. For the gas-phase ion community to be able to utilize excited state emission for the same broad purposes and wide variety of compounds it is used for in the condensed phase, including the excited state charge transfer examples given above, the technique must be made more sensitive. Bringing such studies to the gas phase would confer the advantage of better control of the microenvironment of the fluorophore and more facile comparison with theoretical calculations.

This paper describes a custom mass spectrometer designed for fluorescence spectroscopy of potentially low quantum yield fluorophores. To increase the amount of light collected from the ion cloud, our strategy was to use a linear ion trap, which offers a larger trapping volume than a Paul trap, and light collection optics with a field of view that encompasses the ion cloud. In this scenario, the limiting aperture for light collection is formed by the trapping rods, so the spacing between the electrodes was increased. For convenience, we refer to the trap as the eidLIT for "expanded inscribed diameter linear ion trap." The eidLIT is coupled to a closed-cycle helium refrigerator to enable temperature-dependent studies.

Experimental

COMSOL Simulations of Potential eidLIT Geometries

COMSOL simulations were used to map the stable regions of a-q parameter space for linear ion traps of different rod diameters. The Electrostatics, Electric Currents, and Charged Particle Tracing physics modules were used to create the DC electric field, AC field, and particle trajectories, respectively. The inscribed diameter was fixed at 3.18 mm (0.125″), and rod diameter was set to 1.145, 0.8, and 0.5 times the inscribed diameter. Charged particles assigned a mass of 100 u and one unit of charge were released from a 1.27 mm diameter surface centered on the entrance of the four rods. The particles were released at 11 time points during the first rf cycle, and from 100 spatial points on an evenly spaced grid on the release surface, corresponding to a total number of particles of 1100. The initial velocity of the particles was 1389 m/s in the axial direction, corresponding to 1 eV of kinetic energy, and 0 m/s in the radial direction. Transmission efficiency was determined by dividing the number of particles that passed through a 1.27 mm hole at the exit of the quadrupole by the total number of released particles.

To simulate trapping efficiency, a similar model and the same physics packages were used. In this case, the inscribed diameter was 4.97 mm, particles were released from a 2.48 mm diameter inlet surface, but with 40 different velocity vectors corresponding to 10 eV of kinetic energy for a 443 *m/z* ion, corresponding to the mass-to-charge of rhodamine 6G. The velocity vectors are evenly distributed over a hemisphere so that particles have an assortment of off-axis components to their velocities. A packet of 40 particles was released from 21 spatial points at 11 time points distributed over the first rf cycle, for a total of 9240 particles. Both programs used for the simulations can be downloaded under the "Methods" tab of www.coldions.org.

Sample Preparation, Ion Formation, and Mass Selection Prior to the eidLIT

Rhodamine 6G, purchased from Sigma Aldrich (St. Louis, MO, USA), was used without further purification and diluted to 20 μM concentration in equal parts water and methanol. The sample is injected into the sprayer body from a MicroMass QuattroUltima at a flow rate of 1 μL/min, and nebulized using 40 psi N_2.

Shown in Figure 1 is a cutaway view of the axis of the ion path through our beam/trap mass spectrometer, which is a compilation of in-house built components and a custom configuration quadrupole mass analyzer from ArdaraTech (Ardara Technologies, L.P., Ardara, PA, USA). The system can act as a stand-alone beam type quadrupole mass analyzer, or can be used to transmit a beam of mass-selected ions to the eidLIT for spectroscopy experiments.

Ions formed by electrospray ionization (ESI) are introduced into the first differentially pumped region of the vacuum chamber (1.5 Torr) through a heated capillary, typically set to 140 °C.

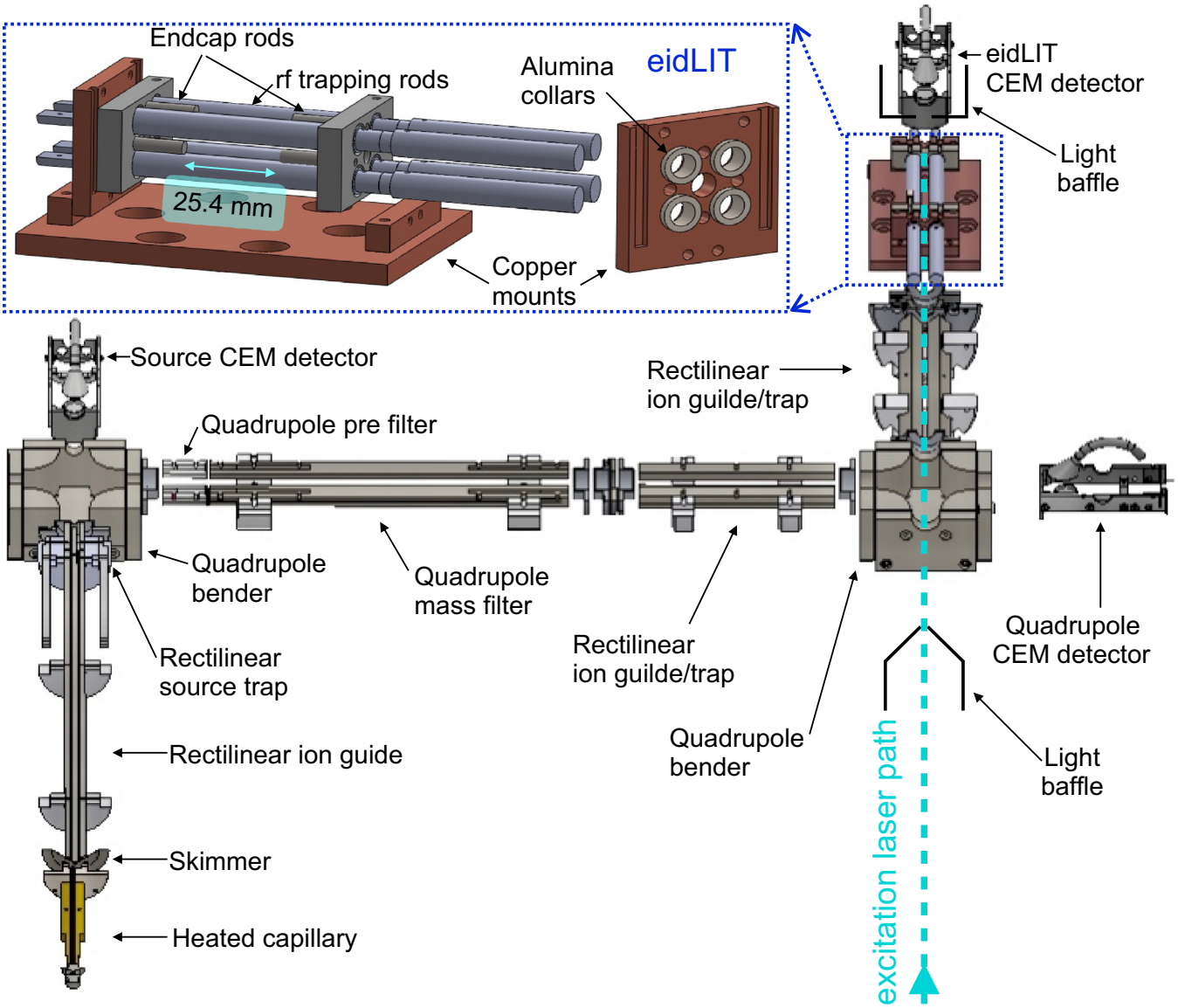

Figure 1. Schematic of the instrument for fluorescence collection. Ions produced using ESI are guided through a series of lenses, rectilinear ion guides, benders, and a quadrupole mass filter to load a linear ion trap designed for temperature and solvation dependent fluorescence spectroscopy. Inset is a SolidWorks model of the eidLIT with one of the electrode mounts removed to show the details. The laser beam enters and exits the eidLIT along the same direction as the ions. Light baffles at the vacuum entrance and before the final CEM detector, used to limit scattered light in the eidLIT chamber, are sketched in to-scale

Alternatively, vaporous neutrals introduced through the heated capillary can be ionized by a glow discharge established between the lens surrounding the capillary exit and the following skimmer. A 1 mm offset between the capillary exit and the 1.8 mm (0.07″) orifice skimmer limits neutral flow into the next differentially pumped region (7×10^{-4} Torr). The exit of the skimmer cone encloses the entrance to a 5.3 mm inscribed diameter rectilinear ion guide that transmits ions into the third differentially pumped region of the vacuum chamber (7×10^{-8} Torr). A 25.4 mm (1″) segment at the end of the rectilinear ion guide is electrically isolated from the main section and has separate DC voltage control so that it can accumulate and store ions. Subsequent to the rectilinear ion trap is a quadrupole bender. Voltages on the bender electrodes can be set either to steer ions to a channel electron multiplier (CEM, DeTech 402A-H) to diagnose ion production from the source, or to bend ions into a quadrupole mass filter.

The quadrupole can act as an ion guide in rf-only mode, be set to transmit a selected *m/z* window, or scanned to obtain a mass spectrum. When scanning the quadrupole, ions are transmitted through the subsequent 13 mm inscribed radius rectilinear quadrupole and bender to the in-line second CEM. Ions can also be trapped in the rectilinear quadrupole to accumulate ions away from the excitation laser path to improve the duty cycle of spectroscopy experiments. The rectilinear ion guide/trap located after the second bender serves to transmit ions into the final differentially pumped vacuum chamber (2×10^{-6} Torr background, 10^{-3} Torr He added) that houses the eidLIT.

Construction and Temperature Control of the eidLIT

The design of our cryogenic linear ion trap (eidLIT) is driven by the goal of maximizing photon collection while operating from ambient to cryogenic temperatures. Radially ions are trapped using round rods constructed from 7.9 mm (5/16″) diameter electropolished 304 stainless steel, positioned around a 9.9 mm inscribed diameter, for a ratio of rod to inscribed diameter (d/d_0) of 0.8. The d/d_0 is smaller than the 1.145 often used to approximate an ideal quadrupole. The transformation can be thought of as either an expansion of the inscribed diameter, hence the shorthand name eidLIT, or equivalently as a reduction in the rod diameter. Axially ions are confined using 4 mm diameter interstitial endcap rods positioned on a 17.2 mm inscribed diameter. The length of the trap between the endcap rods is 25.4 mm.

The eidLIT is mounted to the second stage of a Sumitomo RDK-408D2 closed-cycle helium refrigerator (Janis, Woburn, MA, USA) via copper mounts. Non-porous alumina (McMaster-Carr 8746K18) collars are tight fit to both the rods and the copper mounting blocks to electrically insulate them from grounded surfaces while providing thermal contact to the cold head. Slots cut through the collars allow for the difference in thermal contraction between alumina and copper. The endcaps are mounted off the same copper supports as the trapping rods, and separated by alumina spacers. The copper radiation shield that is mounted on the first stage of the refrigerator, and houses the eidLIT, is also used to precool the wire connections to the eidLIT and the 10^{-3} Torr of helium gas used for trapping. The radial trapping rods of the eidLIT extend beyond the endcaps and out past the radiation shield to collect ions from the previous rectilinear ion guide and transmit them through the radiation shield.

Calibrated silicon diode temperature sensors (Lakeshore DT-670B1-SD) are mounted within a copper block in direct contact with the second stage and on the endcap mounts. The temperature is measured by a LakeShore model 336 temperature controller, which also handles the output to two 50 Ohm heaters inserted into the second stage copper block. The refrigerator can only operate at maximum power; to achieve a temperature above the minimum, the heaters are used to overload the cold head until the setpoint temperature is achieved.

Electronics and Software Control

The electronics supporting the quadrupole mass analyzer and associated ion optics were provided by ArdaraTech. The eidLIT endcaps are powered by TReK power supplies (Entrance: model 601B-4, Exit: model PO641M) set to a range of −500 V to +500 V. An 880 kHz Extrel 150QC is used to provide the rf trapping voltage for the eidLIT. The Extrel 150QC is designed to drive a ~20 pF load, but for the eidLIT the close coupling needed for thermal contact to the grounded cold head results in a 75 pF load for each pair of rods. To bring the load into resonance with the power supply, a capacitive divider and symmetric variable capacitors were used, as shown in Supplementary Information Figure 1. The penalty for the modification is a reduced voltage at the trapping electrodes; a 7 kV output of the Extrel 150QC is required to supply 2 kV to the trapping rods.

Software control and timing of the electronics was accomplished using a custom LabVIEW program developed by Danell Consulting, Inc. Analog command voltages were provided by National Instruments compact data acquisition (compactDAQ) 9264 cards, and a PXI-6723 housed within a PXI-1042 chassis that communicates to the computer via a MXI controller. Digital triggers are handled by a PXI-6229. Current from the CEMs is amplified and converted to a voltage signal in an ArdaraTech preamplifier, and read into the software by the PXI-6229 card.

Laser Excitation, Light collection, and Spectroscopy

The ions are illuminated by a 488 nm continuous wave solid state laser from Spectra Physics (p/n PC14584) that is focused down to a 2 mm $1/e^2$ diameter at the center of the trap. The beam measurement is done outside the vacuum chamber at the same distance from the light's entrance to the center of the trap using a complementary metal-oxide semiconductor camera (ThorLabs DCC1645C). The last focusing element is 600 mm away from the trap center outside the vacuum chamber. The beam travels into vacuum through an anti-reflection coated quartz window, then through a 5 mm diameter hole in the tip of a 45° Aerodag-coated Delrin cone that is press-fit to the viewport flange on the inside of the vacuum chamber to prevent scattered light from permeating the vacuum chamber. The laser enters the eidLIT through the second bender and rectilinear ion guide/trap, along the same direction as the ions. After exiting the trap the beam passes through a 6.35 mm (0.25″) aperture in a 3.18 mm (0.125″) thick aluminum plate blackened with Aerodag, then between the conversion dynode and multiplier cone of the CEM, and exits the vacuum chamber through a second anti-reflection coated quartz window. The exit light baffle has a larger aperture because the ions also pass through it on the way to the CEM, and it is a flat plate instead of a cone so that the CEM can be positioned as near to the eidLIT as possible.

Excitation occurs along the axis of the eidLIT while emission is collected radially. The first element of the light collection optics is a short back focal length (12 mm), high numerical aperture (0.6) aspheric lens (ThorLabs ACL2520U-A), mounted 13.5 mm from the eidLIT axis. The lens is made from B270 optical crown glass, which is opaque in the mid and far infrared, and in thermal contact with the second stage of the cold head, so it is not expected to contribute an additional heat load to the ion cloud. Because the ion cloud is a cylinder whereas the lens has a circular face, the mount is designed to mask the non-illuminated part of the lens to decrease the scatter background. An estimated 8% of the fluorescence emitted from the ion cloud hits the front surface of the first lens.

The collected light passes out of the vacuum chamber through a recessed quartz viewport 60 mm from the trap axis.

After exiting the vacuum chamber the light path is as follows: a 30 mm diameter achromatic doublet (ThorLabs AC300-050-A) is used to improve off-axis light collection and allow for misalignment due to thermal expansion and contraction. An interference band pass filter (Chroma Technology Corp. ET525/50) and a color filter (ThorLabs FGL495) reject scattered light to reduce the background signal. Finally, a matching aspheric lens (ThorLabs ACL2520U-A) focuses the collected light onto the 8 mm aperture of a photomultiplier tube (PMT, Hamamatsu H10721P-210) located 95 mm from the trap axis. All optics and the PMT are mounted within a rigid ThorLabs cage system such that the alignment of optics relative to each other is constrained mechanically, but the system as a whole can be aligned relative to the trap to optimize signal. The current output of the PMT is measured by a picoammeter (Keithley model 485), read into the computer via the general purpose interface bus, and recorded using a LabVIEW program.

An example timing diagram used for characterizing the trap load time and fluorescence signal is shown in Supplementary Information Figure 2. After mass-selected ions are loaded into the eidLIT, the voltage on the entrance endcap of the trap is raised to close the trap, and the source trap exit lens is ramped to accumulate ions. A beam flag is attached to the read-write head of a hard disk to act as a shutter [39]. By supplying 10 V to the voice-coil actuator, the flag is removed from the beam path, opening the shutter so that ions can be irradiated. The actuator is then closed and the trapped ions are dumped to the third CEM detector by raising the voltage on the entrance endcap and lowering the voltage on the exit endcap.

Emission spectra were recorded with an Ocean Optics QEPro spectrometer, which can only collect light delivered through a SM-1 fiber coupler. In place of the achromat-ashpere-PMT assembly described above, a 25.4 mm diameter air-spaced doublet collimator (ThorLabs F810SMA-543) placed on the vacuum chamber window focused light onto a 1.5 mm multimode fiber (ThorLabs FT1500EMT), which then was coupled into the spectrometer. The QEPro can be configured with a number of slit sizes, and 25 μm was used in this case. The detector is a back-thinned and thermoelectric-cooled charged coupled device (CCD) array (Hamamatsu S7031-1006S). OceanView software was used to control the spectrometer and record data. Spectra were integrated for 60 s, and a background spectrum acquired without ions present in the trap was subtracted in software.

Results and Discussion

COMSOL Modeling of LIT Geometries

A 25.4 mm length between the endcap rods was chosen because the widest variety of optics is available in that size. Along the long axis, the limiting aperture is the endcap rods, but not all light emerging from the trap impinges the first collection lens, and so the limiting elements for light collection in that dimension are the optics (Figure 3, top). Along the short axis the trapping rods are the limiting aperture, and all emerging light can be collected and focused (Figure 3, bottom). Adjustments to the trapping rod geometry, then, have the potential to improve light collection efficiency. From a light collection perspective using thin wires as trapping electrodes would be optimal, but it is doubtful that such a device would be a sufficient ion trap. Models were used to attempt to determine the amount of geometry distortion that would support better light collection while minimizing degradation of ion trapping performance.

The results of ion trajectory simulations of $d/d_0 = 1.145$, 0.8, and 0.5 are superimposed on plots of purely quadrupolar Mathieu stability regions in Supplementary Information Figure 3. As expected, the simulations for $d/d_0 = 1.145$ delineate the edges of the Mathieu stability boundaries. In comparison, the simulations for $d/d_0 = 0.8$ and 0.5 show stable ion trajectories for a wider range of parameters outside the Mathieu stability regions, and a more gradual boundary edge. The distorted geometries can introduce higher order fields and spatial harmonics that would likely degrade the mass resolution, though there has been prior work that suggests methods for compensating for such field distortions [40]. The plan for the eidLIT is to perform mass analysis by axial excitation and axial ejection [41], in which case the resolution will not depend on the radial trapping field. Preliminary experiments indicate that the axial excitation and ejection mode are effective in this set-up, but studies on resolution are ongoing.

The above simulations were meant to isolate instability caused by the applied electric field, but because ions are initialized with no off-axis velocity components they are a poor representation of the trapping performance of the different geometries. To test how diminishing rod diameter affects the ability to confine a defocused ion beam, simulations were performed where ions were initialized again with 10 eV of kinetic energy, but this time with velocity vectors evenly distributed over the surface of a hemisphere. The transmission probability as a function of the rf drive voltage for different geometries is shown in Supplementary Information Figure 4. While transmission probability suffers for the smaller diameter rods, the effect is not as pronounced as we were expecting. A hemisphere velocity distribution is far more drastically defocused than what should exist in the instrument, but such a poorly behaved velocity distribution was required to demonstrate an effect. Simulations that used an Einzel lens preceding the quadrupole set to both focus and defocus the ion beam at the entrance of the trap showed a negligible difference in transmission probability between the different geometries.

The eidLIT was built with a $d/d_0 = 0.8$ as a departure from a similar geometry that was proven experimentally in the observation of fluorescence from trapped atomic ions [42]. That instrument used a $d/d_0 = 0.89$, but ions were formed within the trap, which is less demanding than this case where ions are formed externally and injected into the trap. The simulations above and experimental results described below suggest that exploration in the direction of slimmer trapping rods would likely be

fruitful. Other options such as mesh- or wire-based traps [43, 44] could also be considered, though they were not chosen for this instrument because light collection is most efficient from the center of the ion cloud, so our preference was for an electrode structure that kept obstructions as far from the center as possible.

Detection of Fluorescence from Trapped Ions

The current collected from the PMT in the presence and absence of ions in the trap is plotted on a log scale in Figure 2, where it can be seen that the maximum signal of 8 nA is more than 100 times greater than the scatter background. The PMT is operated at a control voltage of 0.6 V, which results in a gain of 2×10^4. The cathode radiant sensitivity at 504 nm is 100 mA/W, indicating that 4 pW or 10^7 photons/s were collected in steady state. Given photon count rates reported in literature [27, 30, 45] we expect to be able to measure the spectra and excited state lifetimes of chromophores with fluorescence quantum yields below 10%.

The performance is in part attributable to the comparatively large number of ions and trap design, but also due to the light collection optic assembly. Fluorescence is collected radially, the ion cloud is cylindrically symmetric, and the optics have round faces, so the efficiency of light collection is different between the two dimensions. They are considered independently in the models shown in Figure 3. Light collection from the short axis of the ion cloud is limited by the gap between the trapping rods (Figure 3, bottom). Along the long axis, however, the light collection optics are limiting (Figure 3, top). A common optical scheme for collimating and then refocusing a diffuse light source is a pair of matched lenses with the source positioned at the focal point of the first lens, and our design is built upon this basic concept. Aspheric lenses can have shorter focal lengths than their spherical counterparts, and their use here enables the first 25.4 mm diameter lens to be positioned only 13.5 mm away from the trap axis. The addition of a 30 mm diameter achromatic doublet improves off-axis light collection. Of the 100 rays in the simulation, 32 are collected by the aspheric condenser pair, whereas 44 are collected when supplemented with the achromatic doublet.

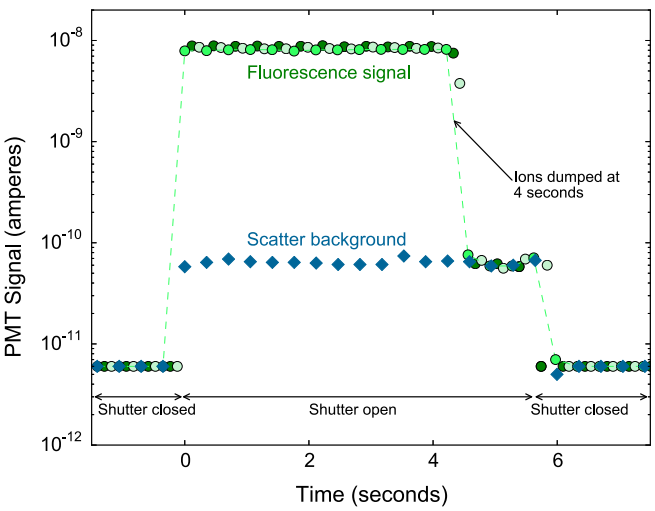

Figure 2. Typical fluorescence and background signal from a fully loaded trap for a laser intensity of 2.2 mW/mm^2 from four consecutive trials. The three sets of data plotted in shades of green indicate the signal in the presence of ions, and the blue represents signal from the scatter background

Outside the vacuum chamber all collection optics are mounted in 8.9 mm thick (non-kinematic) plate mounts. Though the alignment of the optics relative to each other depends on mechanical constraint, an advantage is that they can be placed closer to each other than if 28.4 mm thick kinematic mounts were used. The consequences of the mount choice are that optics with higher lens powers can be used, and that the overall 95 mm beam path is short relative to comparable systems, both of which contribute positively to the photon count rate.

The results of trap loading time experiments are shown in Figure 4 to compare the magnitude of the fluorescence signal with the number of trapped ions. Ions were loaded into the trap for between 0.1 and 120 s, held for 5 s of irradiation, and then ejected to the CEM. The recorded signal from the pulse of ions was integrated as a measure of the number of trapped ions, and the PMT signal during the irradiation time was averaged to yield the PMT signal. During the irradiation time the ions are trapped axially using 50 V on both the entrance and exit endcaps, which according to simulations of the electric field correspond to a maximum axial potential of 10 V on the trap axis between the endcap rods. The kinetic energy of the ions entering the trap is centered around 9 eV (Supplementary Information Figure 5), so after collisions with the helium bath gas the ion cloud should be axially confined to the space between the endcaps. At the 1000 $V_{p\text{-}p}$ drive voltage (q = 0.6) the radial trap depth is calculated to be 19 eV. Saturation of the fluorescence signal indicates that either the ion–laser interaction volume is no longer changing, or that the increase in the ion–laser volume is not observable by the light collection optics. For the most part, the fluorescence signal tracks just ahead of the ion signal, but after approximately 60 s the continued growth of the ion cloud appears to be outside the observable region of the trap.

Persistence of Signal from a Single Trap Fill

The measurement of emission spectra and excited state lifetimes by time correlated single photon counting both require long accumulation times, hence the ability to make long observations from a single trap fill is as useful as a high photon flux. The ability of a $d/d_0 = 0.8$ geometry trap to confine ions for a long period of time was a concern. In addition, dissociation to non-fluorescent product ions would cause a loss of signal, or even worse, dissociation to fluorescent product ions could yield a convoluted spectrum or lifetime. To test the longevity of the experiment, the fluorescence signal was measured as a function of irradiation time for different excitation laser powers (Figure 5b), and compared with the integrated ion signal (Figure 5a). Ions

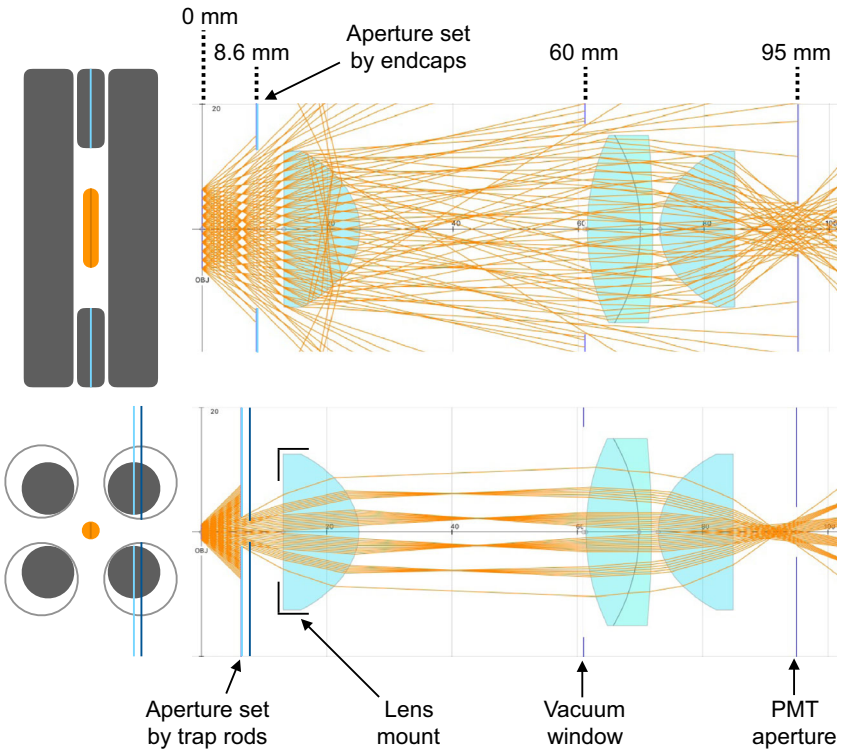

Figure 3. RayLab optical simulations of light collection from the eidLIT. The electrodes (gray) and ion cloud (orange) are sketched to-scale on the left, and indicate the plane of the two-dimensional simulation on the right. The ion cloud is modeled as 10 points along a line at the center of the trap, with 10 rays emitted from each point. The trapping rods and endcaps are modeled as thin apertures at the point of closest constriction, and are highlighted with blue lines on the diagram. The amount of light collected from the long axis (top) is limited by the collection optics. Along the short axis (bottom) the amount of light collected is limited by the gap between the trapping rods. The dark blue lines and open grey circles in the bottom diagram show the dimensions of a $d/d_0 = 1.145$ trap for comparison

were loaded into the eidLIT for a period of 100 s, ensuring that the trap was completely full. They were then irradiated, observed for a variable length of time, and pulsed out to the detector. After 90 s over 80% of the ions are retained in the trap. A decay in the fluorescence signal intensity with

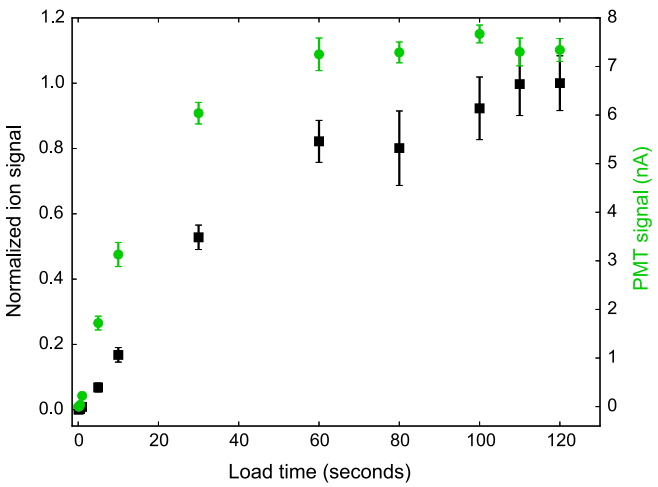

Figure 4. Integrated ion signal (black) and mean fluorescence signal (green) as a function of trap loading time for a laser intensity of 1.2 mw/mm^2. Error bars represent one standard deviation

irradiation can be seen for a laser power density of 1.2 mW/mm^2, but not for the lower laser powers. The flat signal at lower laser powers indicates that the ions lost during the 90 s are from the non-observable region of the trap, which is consistent with the interpretation of the data in Figure 4. Accordingly, the decreasing signal at 1.2 mW/mm^2 is likely due to photodissociation to non-fluorescent product ions.

Rhodamine 6G Emission Spectrum

Although the difference in measured PMT current in the presence and absence of ions is convincing evidence that the observed photons are from emission, a measurement of the spectral attributes of the emission would provide further confirmation. An emission spectrum could also distinguish signal from the parent ions versus fluorescent dissociation products. Because of the relatively high photon flux from the eidLIT, it is also not obvious what caliber of spectrometer is needed to obtain spectroscopic information. The OceanOptics QEPro is a portable, fiber-coupled spectrometer that has the advantages of being rugged, inexpensive, and simple to use. The particular model used had a slit size of 25 µm, corresponding to a wavelength resolution of 1 nm. The detector is a back-thinned, thermoelectric-cooled CCD, which is a relatively sensitive single stage detector. There are, however, multiple stage

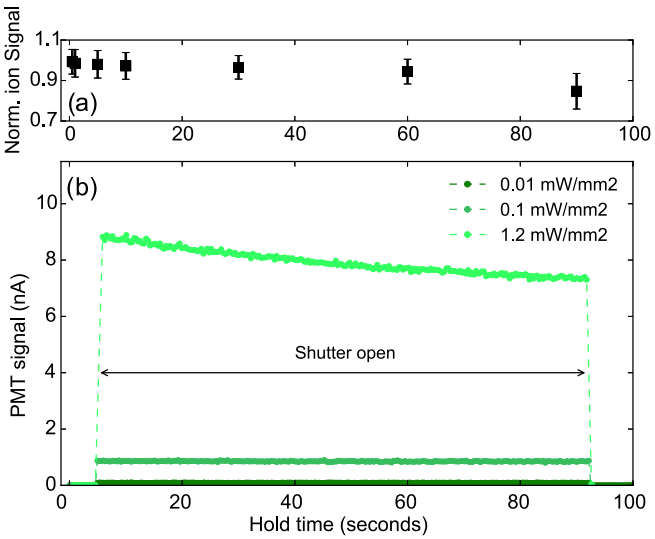

Figure 5. The duration of ion confinement for a fully loaded eidLIT examined both in the absence (**a**) and presence (**b**) of laser light. (**a**) Integrated ion signal as a function of hold time for three trials, error bars indicate one standard deviation. (**b**) Fluorescence observed at the PMT as a function of holding time for different excitation laser intensities

electron multiplied CCD detectors that are much more sensitive to low light conditions, and which are the type used in previous laser induced fluorescence studies on trapped gas-phase molecular ions [45]. Additional losses in sensitivity come from the need to couple light into a fiber. Over 85% of the light collected using the free-space optics described above is lost when coupling into the fiber (Supplementary Information Figure 6). Nevertheless, emission spectra were able to be obtained, and are shown in Figure 6. The figure includes a single background-subtracted spectrum obtained from a 60 s integration time, an average of 25 spectra each corresponding to a separate trap fill, and a 13 point rolling average smoothed spectrum. The profile of the spectrum corresponds to the expected emission of gas-phase rhodamine 6G, as previously reported [45]. The time to acquire the set of spectra was 50 min, so longer averaging is feasible, but the quality of the signal is insufficient to extend the technique to lower quantum yield fluorophores. Nevertheless, the ability to attain a spectrum with such a basic spectrometer is a testament to the number of emitted photons that can be collected from this instrument, and lends confidence in the performance that can be expected from a future spectrometer upgrade.

Cryogenic Capabilities of the eidLIT

The temperature of the eidLIT depends on the equilibrium between the incoming heat load and the ability of the cold head to remove that heat. The specification of the RDK-408D2 refrigerator is that it can remove 20 W of a heat load at 33 K on the first stage, and 1 W of a heat load from the second cooling stage at 4.2 K. The base temperature of our unit under no heat load when tested at the factory was 2.3 K. With the eidLIT installed and operating, the base temperature is 3.5 K at the cold head and 25.5 K at the endcaps (Figure 7).

The heat loads in the system are the radiative heat load of the room temperature vacuum chamber, the conductive heat loads from wire connections at the room temperature vacuum feed throughs, and the convective heat load from introduced gases. The radiative heat load is dumped at the first cooling stage by mounting the eidLIT within a copper box in close thermal contact with the first stage. To bring ions past the radiation shield, the trapping rods are extended 50.8 mm beyond the endcaps and radiation shield to the previous focusing lens. The cost of exposing the portion of the rods outside the radiation shield to room temperature vacuum walls is calculated to be less than 0.1 W. The 10^{-3} Torr of helium used as a trapping gas carries a convective heat load. The gas line feedthrough connects to a copper tube mounted on the first cooling stage to precool the gas before it enters the trapping region, and the expected heat load is also less than 0.1 W. The measured effect of the addition of helium on the temperature, shown in the inset portion of Figure 7, is 0.2 K on the coldhead and 0.4 K at the endcaps. By far the most significant heat load on the trap is attributable to thermal conduction in the in the electrical wires. Manganin wire of American Wire gauge (AWG) size 30 (Lakeshore WMW-30-100) was used between the room temperature vacuum feedthroughs and the first cooling stage. The fine wires are difficult to work with and break easily, so during the prototyping stage, 16 AWG copper was used between the first cooling stage and the trapping rods and endcaps. Replacing the copper wire with manganin would reduce the heat load to the second stage.

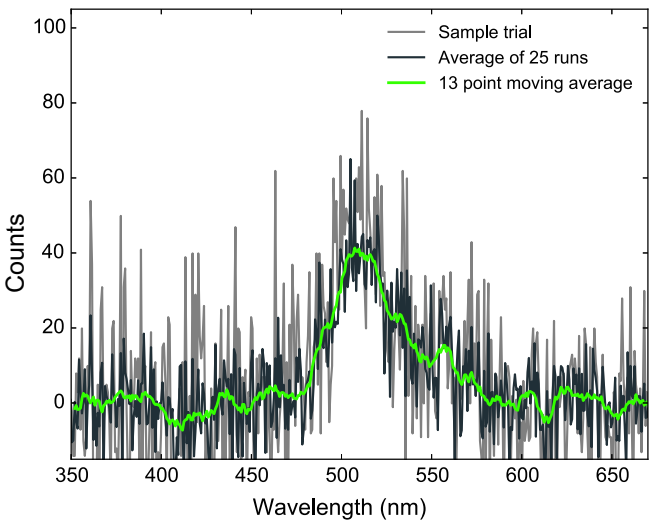

Figure 6. Background subtracted emission spectra of trapped rhodamine 6G ions taken with a hand-held Ocean Optics QEPro spectrometer. The light grey trace is a background-subtracted sample spectrum obtained using a 60 s integration time, the dark grey is the average of 25 spectra, and the bright green is a 13 point moving average smooth. Compared with the collection optics used in Figures 2, 4, and 5, over 85% of the collected light is lost coupling into the fiber required for the spectrometer

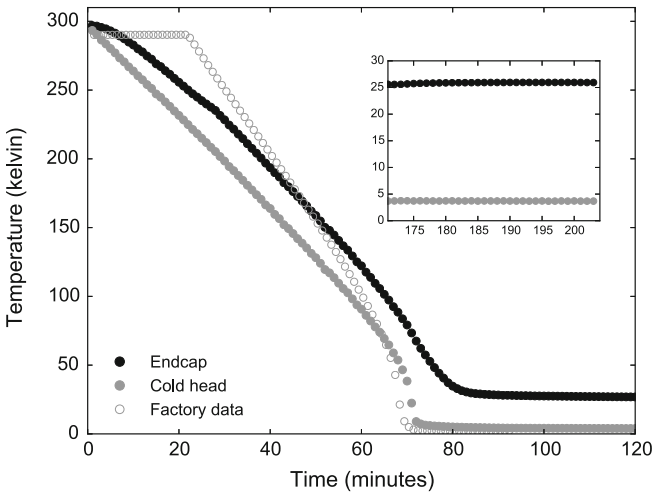

Figure 7. Cryogenic characterization of eidLIT. Temperature of the cold head (black dots) and endcaps (grey dots) is plotted as a function of refrigeration time. The factory data taken under no heat load is shown for comparison (open circles). At 170 min, 1 x 10^{-3} Torr of helium is introduced to the trap (inset plot) when the temperature of the cold head increases from 3.5 to 3.7 K, and the endcaps from 25.5 to 25.9 K, before temperature stabilizes again

Sapphire is the standard material used in cryogenic applications that require thermal conductivity but electrical resistivity. Non-porous alumina has the same chemical formula of sapphire but an amorphous rather than crystalline structure. Specifications of material properties vary widely by purity, manufacturer, and as a function of temperature, but based on material properties quoted by Kyocera and Corning we estimate that alumina has approximately 75% of the thermal conductivity of sapphire. In this case it was used for prototyping because the material is less expensive and readily available, which allowed for design iterations. In the future, the alumina components can be replaced with sapphire for improved thermal performance.

Conclusions

A modified linear ion trap designed for temperature-dependent fluorescence spectroscopy has been constructed and characterized. The eidLIT is coupled to a closed-cycle helium refrigerator, cartridge heaters, and a temperature controller that enable temperature control down to 3.5 K at the coldest and 25.9 K at the warmest parts of the trap. A trap design using a $d/d_0 = 0.8$ was chosen as a balance between gaining optical access to the ion cloud while being confident that trapping efficiency would be maintained. Simulations did indicate, however, that smaller ratios would likely perform sufficiently as an ion trap while increasing the optical access to the ion cloud, and we would encourage work in this direction. To take advantage of the full cylindrical ion cloud, 25.4 mm collection optics were used, but masked to reduce the amount of background scatter collected, and rigidly mounted to achieve the shortest possible light collection path; 10^7 photons/s were detected by a PMT at a signal to noise ratio greater than 100. The eidLIT can sustain an ion cloud large enough for fluorescence signal to be maintained for as long as 90 s provided the excitation laser power is not high enough to cause photodissociation. Both the high photon flux and ability to make long observations will be critical for the measurement of emission spectra and excited state lifetimes of chromophores with low fluorescence quantum yields, which is an improvement needed for the application of gas-phase fluorescence spectroscopy to a wide variety of compounds that undergo reactions from the excited state. The low temperatures will be useful for the formation of chromophore–solvent complexes so that the influence of the microenvironment on excited state chemistry can be studied.

Acknowledgements

The authors express their sincere thanks to Rowland Institute at Harvard for funding this project. Melvin Park, Mark Ridgeway, and Desmond Kaplan of Bruker Daltonics provided helpful discussions, ideas, and equipment donations. Randy Pedder and Chris Taormina of Ardara made excellent improvements during the initial design phase, and provided continued support and insight into their equipment. Don Rogers, Scott Bevis, and Winfield Hill of the Rowland Institute are acknowledged for their contribution to critical elements of the hardware. A special thanks goes to Ryan Danell, whose RITS software enormously simplified day-to-day operations and data collection in the instrument. Joel Parks, Jim Foley, Michael Burns, Lene Hau, and Jene Golovchenko provided an invaluable community and intellectual environment where both broad exploration and refinement of details were encouraged.

References

1. Day, R.N., Davidson, M.W.: The fluorescent protein palette: tools for cellular imaging. Chem. Soc. Rev. **38**(10), 2887–2921 (2009)
2. Rodriguez, E.A., Campbell, R.E., Lin, J.Y., Lin, M.Z., Miyawaki, A., Palmer, A.E., Shu, X., Zhang, J., Tsien, R.Y.: The growing and glowing toolbox of fluorescent and photoactive proteins. Trends Biochem. Sci. **42**(2), 111–129 (2017)
3. Tsien, R.Y.: The green fluorescent protein. Ann. Rev. Biochem. **67**(1), 509–544 (1998)
4. Tomosugi, W., Matsuda, T., Tani, T., Nemoto, T., Kotera, I., Saito, K., Horikawa, K., Nagai, T.: An ultramarine fluorescent protein with increased photostability and pH insensitivity. Nat. Methods **6**(5), 351–353 (2009)
5. Griesbeck, O., Baird, G.S., Campbell, R.E., Zacharias, D.A., Tsien, R.Y.: Reducing the environmental sensitivity of yellow fluorescent protein: mechanism and applications. J. Biol. Chem. **276**(31), 29188–29194 (2001)
6. Mandal, D., Tahara, T., Meech, S.R.: Excited-state dynamics in the green fluorescent protein chromophore. J. Phys. Chem. B **108**(3), 1102–1108 (2004)
7. Litvinenko, K.L., Webber, N.M., Meech, S.R.: Internal conversion in the chromophore of the green fluorescent protein: temperature dependence and isoviscosity analysis. J. Phys. Chem. A **107**(15), 2616–2623 (2003)
8. Kummer, A.D., Kompa, C., Niwa, H., Hirano, T., Kojima, S., Michel-Beyerle, M.E.: Viscosity-dependent fluorescence decay of the gfp chromophore in solution due to fast internal conversion. J. Phys. Chem. B **106**(30), 7554–7559 (2002)
9. Niwa, H., Inouye, S., Hirano, T., Matsuno, T., Kojima, S., Kubota, M., Ohashi, M., Tsuji, F.: Chemical nature of the light emitter of the aequorea

green fluorescent protein. Proc. Natl. Acad. Sci. U. S. A. **93**(24), 13617–13622 (1996)
10. Forbes, M.W., Nagy, A.M., Jockusch, R.A.: Photofragmentation and electron photodetachment from a GFP model chromophore in a quadrupole ion trap. Int. J. Mass Spectrom. **308**(2/3), 155–166 (2011)
11. Westlake, B.C., Brennaman, K.M., Concepcion, J.J., Paul, J.J., Bettis, S.E., Hampton, S.D., Miller, S.A., Lebedeva, N.V., Forbes, M.D., Moran, A.M., Meyer, T.J., Papanikolas, J.M.: Concerted electron-proton transfer in the optical excitation of hydrogen-bonded dyes. Proc. Natl. Acad. Sci. U. S. A. **108**(21), 8554–8558 (2011)
12. Goyal, P., Schwerdtfeger, C.A., Soudackov, A.V., Sharon, H.: Proton quantization and vibrational relaxation in non-adiabatic dynamics of photo-induced proton-coupled electron transfer in a solvated phenol–amine complex. J. Phys. Chem. B **120**(9), 2407–2417 (2016)
13. Blankenship, R.E.: Molecular mechanisms of photosynthesis, 2nd edn. Wiley Blackwell, West Sussex (2014)
14. Heyes, D.J., Hardman, S.J., Hedison, T.M., Hoeven, R., Greetham, G.M., Towrie, M., Scrutton, N.S.: Excited state charge separation in the photochemical mechanism of the light driven enzyme protochlorophyllide oxidoreductase. Angew. Chem. Int. Ed. **54**(5), 1512–1515 (2015)
15. Nogueira, J.J., Corani, A., Nahhas, A., Pezzella, A., d'Ischia, M., Gonzalez, L., Sundstrom, V.: Sequential proton-coupled electron transfer mediates excited state deactivation of a eumelanin building block. J. Phys. Chem. Lett. **8**(5), 1004–1008 (2017)
16. Li, C., Yang, Y., Li, D., Liu, Y.: A theoretical study of the potential energy surfaces for the double proton transfer reaction of model DNA base pairs. Phys. Chem. Chem. Phys. **19**(6), 4802–4808 (2017)
17. Li, G., Guan, S., Marshall, A.G.: Comparison of equilibrium ion density distribution and trapping force in penning, paul, and combined ion traps. J. Am. Soc. Mass Spectrom. **9**(5), 473–481 (1998)
18. Ambrose, P.W., Goodwin, P.M., Jett, J.H., Orden, A., Werner, J.H., Keller, R.A.: Single molecule fluorescence spectroscopy at ambient temperature. Chem. Rev. **99**(10), 2929–2956 (1999)
19. Kondo, T., Chen, W., Schlau-Cohen, G.S.: Single-molecule fluorescence spectroscopy of photo- synthetic systems. Chem. Rev. **117**(2), 860–898 (2017)
20. Huntemann, N., Sanner, C., Lipphardt, B., Tamm, C., Peik, E.: Single-ion atomic clock with 3×10^{-18} systematic uncertainty. Phys. Rev. Lett. **116**, 063001 (2016)
21. Rosenband, T., Hume, D.B., Schmidt, P.O., Chou, C.W., Brusch, A., Lorini, L., Oskay, W.H., Drullinger, R.E., Fortier, T.M., Stalnaker, J.E., Diddams, S.A., Swann, W.C., Newbury, N.R., Itano, W.M., Wineland, D.J., Bergquist, J.C.: Frequency ratio of Al^+ and Hg^+ single-ion optical clocks; metrology at the 17th decimal place. Science **319**(5871), 1808–1812 (2008)
22. Lu, H., Liu, C., Wang, D.-S., Chen, L.-K., Li, Z.-D., Yao, X.-C., Li, L., Liu, N.-L., Peng, C.-Z., Sanders, B.C., Chen, Y.-A., Pan, J.-W.: Experimental quantum channel simulation. Phys. Rev. A **95**, 042310 (2017)
23. Blatt, R., Roos, C.F.: Quantum simulations with trapped ions. Nat. Phys. **8**, 277–284 (2012)
24. Maier, J.P.: Open-shell organic cations: spectroscopic studies by means of their radiative decay in the gas phase. Acc. Chem. Res. **15**(1), 18–23 (1982)
25. Engelking, P.C., Smith, A.L.: Tunable laser fluorescence spectroscopy of the molecular nitrogen cation at 390 nm. Chem. Phys. Lett. **36**(1), 21–22 (1975)
26. Grieman, F.J., Mahan, B.H., Anthony, O.: The laser induced fluorescence spectrum of trapped CD+. J. Chem. Phys. **72**(7), 4246–4247 (1980)
27. Khoury, J.T., Rodriguez-Cruz, S.E., Parks, J.H.: Pulsed fluorescence measurements of trapped molecular ions with zero background detection. J. Am. Soc. Mass Spectrom. **13**(6), 696–708 (2002)
28. Bian, Q., Forbes, M.W., Talbot, F.O., Jockusch, R.A.: Gas-phase fluorescence excitation and emission spectroscopy of mass-selected trapped molecular ions. Phys. Chem. Chem. Phys. **12**(11), 2590–2598 (2010)
29. Friedrich, J., Fu, J., Hendrickson, C.L., Marshall, A.G., Wang, Y.: Time resolved laser-induced fluorescence of electrosprayed ions confined in a linear quadrupole trap. Rev. Sci. Instrum. **75**(11), 4511–4515 (2004)
30. Wang, Y., Hendrickson, C.L., Marshall, A.G.: Direct optical spectroscopy of gas-phase molecular ions trapped and mass-selected by ion cyclotron resonance: laser-induced fluorescence excitation spectrum of hexafluorobenzene ($C_6F_6^+$). Chem. Phys. Lett. **334**(1/3), 69–75 (2001)
31. Dashtiev, M., Zenobi, R.: Effect of buffer gas on the fluorescence yield of trapped gas-phase ions. J. Am. Soc. Mass Spectrom. **17**(6), 855–858 (2006)
32. Sassin, N.A., Everhart, S.C., Dangi, B.B., Ervin, K.M., Cline, J.I.: Fluorescence and photodissociation of rhodamine 575 cations in a quadrupole ion trap. J. Am. Soc. Mass Spectrom. **20**(1), 96–104 (2009)
33. Howder, C.R., Bell, D.M., Anderson, S.L.: Optically detected, single nanoparticle mass spectrometer with prefiltered electrospray nanoparticle source. Rev. Sci. Instrum. **85**(1), 014104 (2014)
34. Stockett, M.H., Houmøller, J., Støchkel, K., Svendsen, A., Nielsen, S.: A cylindrical quadrupole ion trap in combination with an electrospray ion source for gas-phase luminescence and absorption spectroscopy. Rev. Sci. Instrum. **87**(5), 053103 (2016)
35. Danell, A.S., Parks, J.H.: Fret measurements of trapped oligonucleotide duplexes. Int. J. Mass Spectrom. **229**(1/2), 35–45 (2003)
36. Czar, M.F., Zosel, F., Kö nig, I., Nettels, D., Wunderlich, B., Schuler, B., Zarrine-Afsar, A., Jockusch, R.A.: Gas-phase FRET efficiency measurements to probe the conformation of mass- selected proteins. Anal. Chem. **87**(15), 7559–7565 (2015)
37. Shi, X., Duft, D., Parks, J.H.: Fluorescence quenching induced by conformational fluctuations in unsolvated polypeptides. J. Phys. Chem. B **112**(40), 12801–12815 (2008)
38. Nagy, A.M., Talbot, F.O., Czar, M.F., Jockusch, R.A.: Fluorescence lifetimes of rhodamine dyes in vacuo. J. Photochem. Photobiol. A **244**, 47–53 (2012)
39. Maguire, L., Szilagyi, S., Scholten, R.: High performance laser shutter using a hard disk drive voice-coil actuator. Rev. Sci. Instrum. **75**(9), 3077–3079 (2004)
40. Zhao, X., Xiao, Z., Douglas, D.: Overcoming field imperfections of quadrupole mass filters with mass analysis in islands of stability. Anal. Chem. **81**(14), 5806–5811 (2009)
41. Hashimoto, Y., Hasegawa, H., Baba, T., Waki, I.: Mass selective ejection by axial resonant excitation from a linear ion trap. J. Am. Soc. Mass Spectrom. **17**(5), 685–690 (2006)
42. Rajagopal, V., Marler, J.P., Kokish, M., Odom, B.C.: Trapped ion chain thermometry and mass spectrometry through imaging. Eur. J. Mass Spectrom. **22**(1), 1–7 (2016)
43. Wang, L., Xu, F., Dai, X., Fang, X., Ding, C.: Development and investigation of a mesh-electrode linear ion trap (ME-LIT) mass analyzer. J. Am. Soc. Mass Spectrom. **25**(4), 548–555 (2014)
44. Jasık, J., Zabka, J., Roithova, J., Gerlich, D.: Infrared spectroscopy of trapped molecular dications below 4 K. Int. J. Mass Spectrom. **354**, 204–210 (2013)
45. Forbes, M.W., Jockusch, R.A.: Gas-phase fluorescence excitation and emission spectroscopy of three xanthene dyes (rhodamine 575, rhodamine 590, and rhodamine 6g) in a quadrupole ion trap mass spectrometer. J. Am. Soc. Mass Spectrom. **22**(1), 93–109 (2011)